GSI

GSI-94-52
PREPRINT
August 1994

BETA-DECAY OF ^{20}Mg

A. Piechaczek, M. F. Mohar, R. Anne, V. Borrel, B. A. Brown,
J. M. Corre, D. Guillemaud-Mueller, R. Hue, H. Keller,
S. Kubono, V. Kunze, M. Lewitowicz, P. Magnus, A. C. Mueller,
T. Nakamura, M. Pfützner, E. Roeckl, K. Rykaczewski,
M. G. Saint-Laurent, W.-D. Schmitt- Ott, O. Sorlin

(Submitted to Nuclear Physics A)

Gesellschaft für Schwerionenforschung mbH
Postfach 110552 · D-64220 Darmstadt · Germany

Beta-Decay of ^{20}Mg

A. Piechaczek [a], M. F. Mohar [a], R. Anne [b], V. Borrel [c], B. A. Brown [d], J. M. Corre [b], D. Guillemaud-Mueller [c], R. Hue [b], H. Keller [a], S. Kubono [e], V. Kunze [f], M. Lewitowicz [b], P. Magnus [g], A. C. Mueller [c], T. Nakamura [h], M. Pfützner [i], E. Roeckl [a], K. Rykaczewski [i], M. G. Saint-Laurent [b], W.-D. Schmidt-Ott [f], O. Sorlin [c]

[a] *Gesellschaft für Schwerionenforschung, D-64220 Darmstadt, Germ ny*

[b] *GANIL, B.P.5027, F-14021 Caen Cedex, France*

[c] *Institut de Physique Nucléaire, IN2P3-CNRS, F-91406 Orsay Cedex, France*

[d] *Michigan State University, East Lansing, Michigan, USA*

[e] *Institute of Nuclear Studies, University of Tokyo, Japan*

[f] *II. Physikalisches Institut, Universität Göttingen, D-37073 Göttingen, Germany*

[g] *Department of Physics, University of Washington, Seattle, USA*

[h] *Department of Physics, University of Tokyo, Japan*

[i] *Institute of Experimental Physics, University of Warsaw, Poland*

Abstract: The β-decay of ^{20}Mg was investigated. A secondary beam of ^{20}Mg ions, produced in reactions between a 95 A $\times$ MeV ^{24}Mg-beam and a $^{nat.}$Ni-target, was isotopically separated by means of the LISE3 spectrometer at GANIL. This secondary beam was implanted into a silicon detector array surrounded by germanium γ-detectors. The β-delayed proton and γ-ray data, measured for this short-lived nucleus ($T_{1/2} = 95 \pm 3$ ms), were incorporated into an improved ^{20}Mg $\rightarrow$ ^{20}Na decay scheme. The 2645 keV level in ^{20}Na is of importance for the breakout from the astrophysical hot CNO-cycle and the onset of the rapid proton capture process via the reaction ^{19}Ne$(p,\gamma)^{20}$Na. An upper limit of 0.1% for the β-decay feeding of the 2645 keV level and a lower limit for the corresponding log ft value of 6.24 were determined. The implications of this result for the spin and parity assignment of the 2645 keV state are discussed. Concerning the isobaric multiplet mass equation no significant deviation from its quadratic form was found. By comparing the ^{20}Mg β-decay into the proton-unbound 3001 keV state in ^{20}Na and the isospin-mirrored decay into the particle-bound 3488 keV level in ^{20}F, an asymmetry $ft^+/ft^- - 1 = 1.69^{+0.86}_{-0.65}$ was observed.

Preprint submitted to Nuclear Physics A *19 August 1994*

The comparison of the experimentally determined B(GT) values for the Gamow-Teller β-decay of ^{20}Mg with a calculation performed in a full sd-shell model space yields an overall quenching of the Gamow-Teller strength of 0.84, corresponding to an observed fraction of 71% of the calculated strength. The measured Gamow-Teller strength above excitation energies of 3 MeV is more fragmented than predicted by the shell-model calculation.

1. Introduction

The present study of the ^{20}Mg β-delayed proton decay (βp-decay) was mainly motivated by the astrophysical problem of the breakout from the hot CNO (HCNO)-cycle. In 1981 Wallace and Woosley [1] proposed a breakout reaction from the HCNO-cycle, which would ignite the hydrogen burning of nuclei in the Ne-Na cycle and would lead, following a path on the proton-rich side of the valley of stability, to the formation of heavy elements, possibly up to the tin region. This so-called rp-process is expected to occur in hot ($T \geq 5 \times 10^8$ K) and dense ($\rho \geq 5 \times 10^3$ g/cm^3) stellar environments, the initial reaction sequence being ^{15}O$(\alpha,\gamma)^{19}$Ne$(p,\gamma)^{20}$Na. While the (α,γ)-reaction seems to be well understood [2], there are considerable uncertainties concerning the rate of the resonant part of the (p,γ)-reaction. This rate depends on the nuclear structure of the ^{19}Ne and ^{20}Na levels involved, particularly on the properties of the first unbound ^{20}Na level at 2645 keV. In the case of a 1^+ assignment to this state, as reaction studies [3–7] suggest, it would give rise to an s-wave resonance in the (p,γ) reaction and would influence strongly the astrophysical reaction rate. Furthermore, the quantitative understanding of the rate of the resonant ^{19}Ne$(p,\gamma)^{20}$Na reaction requires the knowledege of the quantity $\omega\gamma$, which is defined as

$$\omega\gamma = \frac{2J+1}{(2J_1+1)(2J_2+1)} \times (\Gamma_\gamma \Gamma_p)/(\Gamma_\gamma + \Gamma_p). \qquad (1)$$

J_1 and J_2 denote the spins of the projectile and the target nucleus, J the spin, and Γ_γ and Γ_p the γ- and proton-widths of the resonant 2645 keV level in ^{20}Na. It is clear from eq. (1) that the astrophysical reaction rate depends on the detailed properties of this level. However, the $J^\pi = 1^+$ assignment for the 2645 keV level has been questioned by several authors (see [8] and references therein).

In principle the study of the ^{20}Mg β-decay offers a way to clarify the configuration of the 2645 keV level in ^{20}Na. As the allowed Gamow-Teller (GT) β-decay of the $J^\pi = 0^+$ mother state proceeds to 1^+-states in ^{20}Na, the 2645 keV level would be strongly populated if it had indeed $J^\pi = 1^+$. Correspondingly, the properties of this level and its decay, in particular the ratio Γ_γ/Γ_p, could be studied. Taking Γ_p from calculations, Γ_γ could be determined from the measured ratio Γ_γ/Γ_p and $\omega\gamma$ could then be deduced from eq. (1).

In addition to this astrophysical motivation, it is a challenge to perform a more detailed decay study of the exotic nucleus ^{20}Mg as compared to the previous ones [9–12]. It would allow one to investigate the GT quenching in β-decay, to test the isobaric mass multiplet equation, and to probe isospin symmetry in β-transitions of mirror decays.

After a description of the experimental techniques in the next section, the results of the measurements will be presented in section 3. Section 4 includes the discussion of the astrophysical as well as the nuclear physics aspects mentioned above. Summary and outlook are given in section 5. Preliminary results from this work have already been presented as conference contributions [13–15].

2. Experimental Techniques

The LISE3 facility [16–18], which consists of a zero-degree achromatic recoil spectrometer and a Wien-type velocity filter, was used to produce a monoisotopic radioactive beam of ^{20}Mg. A primary ^{24}Mg beam from GANIL with an energy of 95 A $\times$ MeV impinged upon a 274 mg/cm^2 thick $^{nat.}$Ni target. Nickel was chosen as target material for the production of proton-rich secondary beams with reference to earlier reaction work performed at GANIL, e.g. [19]. Based on the semiempirical systematics EPAX [20] a production cross-section of 0.7 mb for ^{20}Mg was calculated [21]. The LISE3 spectrometer was operated in an achromatic mode with an intermediate degrader of 312 mg/cm^2 $^{nat.}$Al, corresponding to a thickness-to-range ratio of 0.308 for the produced ^{20}Mg atoms. The momentum acceptance of the LISE3 spectrometer was limited to 0.88% at the intermediate focal plane in order to suppress isotonic contaminants which cannot be reduced by the intermediate degrader [22]. The resulting ^{20}Mg abundance of the secondary beam in front of the velocity filter amounted to appoximately 80%. By adjusting the transmitted velocity regime of the velocity filter to the maximum of the ^{20}Mg velocity distribution, the intensity of contaminating isotopes was further reduced to 2.4%.

The ^{20}Mg activity was implanted into the detector array shown in Fig. 1. The secondary beam of ^{20}Mg-ions was implanted into a position-sensitive silicon strip detector (implantation detector), consisting of 16 segments of 5 $\times$ 35 mm^2 area each. The implantation detector of 300 μm thickness was inclined with respect to the beam axis by an angle of 45^0, resulting in an effective thickness of 424 μm in beam direction, which facilitated the complete implantation of the desired activity. The implantation detector was mounted between two segmented large area silicon detectors of 500 μm thickness for the detection of β-rays. As will be shown below, the knowledge of the β-ray kinematics and their energy loss in the β-detectors allows a reduction of the β-energy summing effects in the particle spectra of the implantation detector. A circular silicon detector of 28 mm diameter and 300 μm thickness (energy-loss detector) was used for the isotope identification. In front of this detector a stack of movable aluminum foils served to shift the implantation profile of ^{20}Mg ions into the appropriate position within the implantation detector. This set-up was surrounded by three large-volume germanium-detectors, whose efficiency with respect to a 3" $\times$ 3" NaI-crystal for 1.3 MeV γ-radiation amounted to 70% for the lateral detectors and 35% for the backward detector.

The ^{20}Mg activity was implanted into the central region of the implantation detector with a calculated total width of the implantation profile of about 200 μm. The on-line isotopic identification of the activity arriving at the final focal plane was performed by means of the energy-loss time-of-flight method (see Fig. 2, upper part). The energy loss detector, which also gave the start signal, was situated close to the final focal plane. The stop signal for the determination of the flight time through the spectrometer was supplied by the radiofrequency of the accelerating cyclotron. As can be seen from Fig. 2, ^{20}Mg with an abundance of 97.6% is clearly separated from the isotonic contaminants ^{18}Ne, ^{17}F and ^{16}O, whose relative intensities amount to 1.9%, 0.19%, and 0.04%. ^{19}Na is proton-unbound and

obviously not transmitted through the spectrometer. It should be noted that during part of the experiment the relative purity of the transmitted ^{20}Mg reached 99.6%. The rate of ^{20}Mg atoms arriving at the implantation detector varied between 30 and 150 atoms/s with a continuous primary beam.

The influence of secondary reactions during the implantation process is demonstrated in the lower part of Fig. 2. Shown is the pulse height in the energy-loss detector versus the pulse height of the implantation detector for those ions that were identified as ^{20}Mg in the upper part of Fig. 2. Four classes of events can be distinguished (abundances are given in parentheses), namely

(i) ^{20}Mg atoms, which did not undergo a secondary reaction (96.6%),
(ii) products of secondary reactions which occurred in the implantation- or β-detectors or in the stack of aluminum foils (2.6%),
(iii) products of secondary reactions which occurred in material in front of the energy loss detector (0.4)%,
(iv) events of unknown origin (0.1%).

The purity of ^{20}Mg atoms in the implantation detector amounts to (94.3 ± 0.5)%. During the experiment a total number of 4.5×10^6 ^{20}Mg atoms was implanted.

3. Results

3.1. β-Delayed Particle-Spectra

Fig. 3 shows the spectra of decay events in the six central segments of the implantation detector. High-energy implantation events ($\approx$ 200 MeV total energy) are absent in these spectra since they were recorded in anticoincidence with the energy-loss detector. The lines marked as $\alpha_1 \cdots \alpha_9$ were identified as $\beta\alpha$-activity from the decay of the daughter activity ^{20}Na [23,24]. The remaining lines, denoted as $p_1 \cdots p_{11}$, were ascribed to the βp-decay of ^{20}Mg. This assignment was confirmed by a halflife analysis in the case of the strongest lines p_1, p_4, p_{10}, and p_{11}. A compilation of the proton-lines observed in this experiment is given in Table 1.

The abscissa of the spectra shown in Fig. 3 is the total energy deposited in the implantation detector. It is roughly calibrated on the basis of the most prominent ^{20}Na $\beta\alpha$-lines denoted as α_2 and α_7. Spectrum (a) was obtained without any coincidence requirement with respect to the β-detectors. Spectrum (b) was recorded in coincidence with β-rays in a segment of a β-detector opposite the strip of the implantation detector where the decay-event occurred. This condition selects short path lengths of the emerging high-energetic β-ray in the material of the implantation detector which leads to a reduced energy deposition in this detector and hence to a reduction of β-energy summing. This can be clearly seen e.g.

in the improvement of the peak-to-valley ratio at the low-energy side of the proton line denoted as p_5. As can be seen from spectrum (c), a further improvement can be obtained by imposing an additional condition on a small energy loss of the β-rays in the β-detector, which also corresponds to a small β-energy loss in the implantation detector.

Fig. 4 shows the low energy part of the pulse-height spectrum measured in the implantation detector. This spectrum was recorded in coincidence with a β-ray in a segment opposite to the strip where the βp-decay occured in order to suppress the β-background and in anti-coincidence with the backward germanium-detector in order to eliminate contributions from light beam-induced particles in the spectra. Since the proton separation energy of ^{20}Na amounts to 2195 $\pm$ 7 keV [25], the proton line from the βp-decay of the 2645 keV level in ^{20}Na is expected to occur at a proton energy of 450 keV. No significant structure is seen at this position. As the shape of the expected proton line is known from transitions with higher proton energies, an upper limit of 0.1% was estimated for the β-feeding of the 2645 keV level and its subsequent proton decay by comparing the expected peak heights for various branching ratios with the measured spectrum.

Besides the measurement with continuous beam, a measurement with a pulsed beam was carried out. During a period of 200 ms ^{20}Mg ions were implanted, whose decay was recorded in the following 800 ms intervall. From those pulsed-beam data, a spectrum exclusively containing the proton radioactivity from the ^{20}Mg decay (see Fig. 5) was constructed in the following way: From the data taken during the 800 ms beam-off period the part accumulated in the time interval $100 \leq t \leq 800$ ms was subtracted. The subtracted spectrum, which mainly contains the longer lived ($T_{1/2} = 447.9 \pm 2.3$ ms [24]) ^{20}Na activity, was scaled by a factor, so that in the resulting difference spectrum the prominent, isolated ^{20}Na α-line α_7 at 5540 keV disappeared. The shape of the low-energy β-background was determined by gating on the 984 and 1634 keV γ-rays from the ^{20}Mg and ^{20}Na $\beta\gamma$-decay. The additional subtraction of the β-background yielded the proton spectrum displayed in Fig. 5. The energies marked by arrow symbols in Fig. 5 correspond to proton lines attributed to the ^{20}Mg precursor on the basis of the spectra displayed in Fig. 3. Due to the limited statistics, only some βp-lines observed in the continuous-beam measurement were confirmed by the pulsed-beam experiment. In the proton energy range between 2 and 4 MeV a continuum of unresolved transitions is observed, which cannot be explained by the effect of summation between β-energy loss and proton energy deposition.

3.2. γ-Spectra

Fig. 6 shows a γ-spectrum which stems from decay events of the implanted activity. The spectrum was taken in anticoincidence with the energy-loss detector in order to suppress γ-rays from nuclear reactions during the implantation process. Room background was suppressed by requiring a coincidence with a decay-event in the implantation detector. A detection efficiency of $\varepsilon_\beta = (58.8 \pm 1.2)$ % for β-rays from the implanted activity was determined by comparing the number of recorded 1634 keV γ-rays and 5540 keV

α-particles, which originate both from the decay of ^{20}Na and have well known branching ratios [23,24]. The detection efficiency for β-delayed γ-radiation from implanted activity $\varepsilon_{\beta\gamma}$ was obtained as $\varepsilon_{\beta\gamma} = \varepsilon_\beta \times \varepsilon_\gamma$, where ε_γ denotes the absolute γ-ray detection efficiency as determined by employing standard calibration sources. No further correction was performed to obtain the detection efficiency for proton-coincident γ-rays $\varepsilon_{p\gamma}$, since the detection efficiency for protons from the implanted activity was assumed to be 100% on account of the high energy loss per unit length for protons as compared to positrons. The effects of γ-ray summing due to cascading γ-rays or 511 keV annihilation radiation were estimated by using the GEANT [26] computer code to be in the order of 10%. This summing probability was taken into account for the determination of branching ratios by evaluating the γ-data.

The spectrum displayed in Fig. 6 shows γ-rays from the $\beta\gamma$-decay of ^{20}Mg (984.25 keV), and ^{20}Na (1634 keV), as well as γ-rays following the βp-decay of ^{20}Na into excited states of ^{19}Ne at 238, 275, 1508, and 1536 keV. The $\beta\gamma$-rays of the ^{20}Mg decay were observed for the first time in this experiment. The β-decay branching ratio b_γ for the 984 keV-level was determined to be $b_\gamma = 0.705 \pm 0.014$ from the γ-data, but see Sect.3.4. The γ-line at 1041 keV stems from the implanted contaminant ^{18}F. All other lines in the spectrum were assigned to 511 keV-quanta and summing or escape events.

Gamma-lines from the decay of the 2645 keV level in ^{20}Na were searched in the measured γ-ray spectrum under two different assumptions:

(i) If the level at 2645 keV was the analogue state of the 3173 keV, (1^+)-level in ^{20}F, one would expect that the predominant radiative decay of the 2645 keV state proceeds to a not yet observed 1^--level at approximately 980 keV excitation energy, corresponding to a γ-line of about 1665 keV,
(ii) If the 2645 keV level was the analogue state of the 2966 keV, 3^+-level in ^{20}F, one would expect that the deexcitation of the 2645 ± 6 keV level would populate the states at 0, 596 ± 8, and 802 ± 7 keV excitation energy, yielding γ-lines at 2645 ± 6, 2049 ± 10, and 1843 ± 9 keV.

For both cases no γ-lines have been observed in the respective energy regions. The resulting upper limit for the population of the 2645 keV level by the β-decay of ^{20}Mg and its subsequent γ-deexcitation was determined to be 1.0%. From the decay properties of the 3488 keV level in ^{20}F the γ-deexcitation of its analogue state in ^{20}Na at 3001 ± 2 keV is expected to proceed to the levels at 0, 984.25 ± 0.1 , 1346 ± 8, and 1837 ± 7 keV, yielding transition energies of 3001, 2017 ± 2, 1655 ± 8, and 1164 ± 7 keV. Again, the corresponding γ-lines have not been observed. This will be of importance for the discussion of isospin asymmetries in Sect. 4.3.

3.3. *Half-Life of ^{20}Mg*

For the determination of the half-life of ^{20}Mg the pulsed-beam measurement as described in Sect. 3.1 was used. The ^{20}Mg half-life was determined in two ways by evaluating the β-delayed proton activity:

(i) The decay of the proton line p_4 at 1675 keV was fitted by a one-component exponential function resulting in a half-life of 96 $\pm$ 3 ms with a reduced χ^2-value of 0.75. This line has essentially no background from the $\beta\alpha$-decay of the daughter activity ^{20}Na.
(ii) For the decay of the proton line p_1 at 802 keV a background due to low energy β-activities (^{20}Na, ^{18,19}Ne and ^{17}F), which show a decay different from that of ^{20}Mg, was subtracted. The shape of the subtracted background was determined from a proton energy region close to the 802 keV proton line, the amount of background was determined from the requirement that the remaining activity (i.e. ^{20}Mg) must represent a purely exponential decay. The best exponential fit obtained resulted in a half-life of 94 $\pm$ 4 ms with a reduced χ^2-value of 0.83.

The weighted mean value, obtained from methods (i) and (ii) amounts to $T_{1/2} = 95 \pm 3$ ms. This value of the ^{20}Mg half-life agrees with previous measurements of 95^{+80}_{-50} ms [9] and 114 $\pm$ 17 ms [11] within the respective error bars but is considerably more accurate than those results. However, it is in disagreement with the value of 82 $\pm$ 4 ms reported in ref. [12]. As will be seen from the data presented in section 4.4, the latter result has to be questioned as it corresponds to an unreasonably large Fermi transition strength.

3.4. *^{20}Na Level Energies and ^{20}Mg Decay Scheme*

From the measured particle-, γ-, and particle-γ coincidence-spectra a partial $^{20}\mathrm{Mg} \rightarrow {}^{20}\mathrm{Na}$ decay scheme was derived (see Fig. 7). The full information obtained in this experiment about γ-, β- and βp-branching ratios as well as ^{20}Na excitation energies is compiled in Table 2. All the branching ratios given in Table 2 are normalized to the number of decaying ^{20}Mg atoms as 100%.

The β-branching ratio b_p into proton unbound levels in ^{20}Na was determined by using the following relations:

$$N_p + N_\alpha = N_{Mg} \times b_p + N_{Mg} \times (1 - b_p) b_\alpha \qquad (2)$$

and

$$N_{Na} = N_{Mg} \times (1 - b_p), \qquad (3)$$

where N_p, N_α and N_{Mg} denote the number of measured protons, α-particles and ^{20}Mg-atoms, and b_α indicates the branching ratio for $\beta\alpha$-emission from ^{20}Na. The advantage of this method is that no decomposition of the particle spectra into a proton- and α-part is necessary, which is difficult with β-summing effects. Using the quantities measured in this experiment and $b_\alpha = 0.1998 \pm 0.0134$, determined from ref. [24], a value of $b_p =$

0.303 ± 0.012 is obtained. This value of b_p together with the $\beta\gamma$ branching-ratio b_γ of 0.705 ± 0.014 as determined from the γ-data for the decay to the 984 keV bound level results in a total branching ratio for the ^{20}Mg decay of 1.008 ± 0.018, indicating that the intensity balance is fulfilled within the experimental uncertainty limits. We adopted a value $b_\gamma = 1 - 0.303 = 0.697$ instead of 0.705, since the last value is slightly biased by the assumption of an energy-independent β-detection efficiency of the implantation detector (see Sect. 3.2).

Fig. 8 shows the proton spectra of the ^{20}Mg βp-decay, in which the proton emitted from ^{20}Na populates one of the first four excited states in ^{19}Ne at 238, 275, 1508, and 1536 keV excitation energy. The spectra were obtained from $p\gamma$-coincidence data by using the known decay properties of the excited ^{19}Ne levels to correct for the effects of cascading γ-rays. Negative numbers of counts are caused by the subtraction of background events. The significance of the observed structures can be judged from the almost complete disappearance of the strong ^{20}Na α-line at 5540 keV (see Fig. 3). Besides several peaks broad or unresolved structures are observed around ^{20}Na excitation energies of 4800 and 5600 keV.

For the evaluation of the βp branching ratios of the ^{20}Mg decay from the particle spectra of the implantation detector the detection efficiency of this counter for protons and α-particles was assumed to be 100%. However, a correction for incomplete proton-energy deposition had to be made. The percentage of protons which do not fully deposit their energy in the detector was determined as a function of the proton energy by using the GEANT computer code. The spatial distribution of the implanted activity along the beam axis, which influences the proton escape probability, was calculated by means of the LISE program [27]. For protons with kinetic energies of 4.3 MeV (corresponding to an IAS $\rightarrow$ ^{19}Ne g.s. transition) the correction due to escape events amounted to 15%.

The branching ratio of βp-emission into excited states of ^{19}Ne $b_p^{exc.} = 0.0695 \pm 0.008$ was obtained from the ratio between the number of counts in the four spectra shown in Fig. 8 and the number of implanted ^{20}Mg atoms. From this value and the value $b_p = 0.303 \pm 0.012$ the total βp-decay branching ratio into the ^{19}Ne ground state was determined to be $b_p^{g.s.} = 0.2335 \pm 0.015$. From the spectra displayed in Fig. 8, branching ratios for the β-decay of ^{20}Mg into individual excited states of ^{20}Na and the subsequent p-decay into individual levels in ^{19}Ne were determined (3rd to 7th column in Table 2).

The ^{20}Na level energies for proton-unbound states given in Fig. 7 and Tables 1 and 2 were determined in the following way: One calibration point was obtained from the energy of the ^{20}Na level around 3 MeV, which was determined as the weighted mean value of previous measurements to be 3001(2) keV (see Table 3 for references). The pulse-height defect of the recoiling ^{19}Ne atoms was treated within the framework of the LSS-theory of nuclear stopping [28–30], since a comparison of LSS theory and measurements of the pulse-height defect for neon- and other light nuclei [31–37] showed that the LSS-theory describes the pulse-height defect in the relevant energy range with an accuracy of approximately 10 keV. The slope of the energy calibration was determined from the difference between the

proton line from the IAS decay to the ^{19}Ne groundstate and the 1536 keV level in ^{19}Ne. Different endpoint energies of the emitted β-rays and consequently different energy losses of the β-rays in the implantation detector correspond to the β-transitions into the various excited ^{20}Na levels. This leads to an energy dependence of the β-energy summation to the lines in the proton energy spectra and to a shift of the observed proton lines, which depends on the excitation energy of the proton-emitting level. This effect, which is in the order of 80 to 100 keV, was also corrected by using the GEANT computer code. The good agreement between the energy of the IAS determined in this experiment as 6521 $\pm$ 30 keV with the value of 6533 $\pm$ 13 keV from ref. [12] proves the validity of the described method to obtain the ^{20}Na excitation energies.

Table 3 represents a compilation of ^{20}Na level energies and J^{π}-values obtained in this and other experiments. Levels determined from different authors were assumed to be identical if their excitation energies agreed within the error bars. The last column of Table 3 shows the weigthed mean excitation energies and the J^{π} assignments which are compatible with the experimentally determined J^{π}-values. In most cases there is agreement between the different measurements so that at least tentative J^{π}-assignments can be given. Ambiguities occur in the case of a 3035 $\pm$ 15 keV-level from ref. [6], which could be identified either with the level at 3001 keV or with that at 3067 keV. A level observed at 3100 $\pm$ 14 keV [6] was not confirmed by a later measurement [7]. Both states were omitted in the compilation as well as in the calculation of the average excitation energies. The grouping of the level at 5430(60) keV together with the broad level around 5600 keV is somewhat arbitrary.

4. Discussion

4.1. Astrophysical Aspects

The nature of the 2645 keV-level in ^{20}Na has been in question for a long time. As can be seen from Table 3, reaction studies suggest this state to be 1^+ [3–7]. Accordingly, one would expect the level to be populated in the β-decay of ^{20}Mg with a log ft value of about 4, as can be estimated from the log ft values of other levels populated in the present experiment (cf. the values given in Table 6). However, we measured a lower limit for the log ft value of the β-decay to this state of 6.24, which represents the most stringent log ft limit determined for this level so far. This contradiction could be solved by the assumption that the 2645 keV level in ^{20}Na is a $2\hbar\omega$ intruder state, which has a configuration such as $p^{-2}(sd)^6$ [6,7,11] or a structure $(1s^{-1}2s^1)$ or $(1p^{-1}2p^1)$ with almost no $(sd)^4$ component [12]. Such a state is predicted by shell modell calculations in the A = 20 system at an excitation energy around 3 MeV [39]. Indeed for the 3173 level in ^{20}F, which is tentatively assigned as 1^+, indications exist that it carries little $(sd)^4$-strength, e.g. that it is not populated in the thermal neutron capture of ^{19}F [38] or in the β-decay of ^{20}O (log ft $\geq$ 5.08) [39].

Furthermore, the 3173 keV level decays predominantly to the 984 keV, 1^--level, as it would be expected for a $2\hbar\omega$ intruder state in contrast to the more complex decay of the 3488 keV level, which has a dominant $(sd)^4$-structure. On the other hand the known decay behaviour of the 3173 keV level could also support a $J^\pi = 0^-$ assignment for this level [40]. Clearly the 2645 keV level in ^{20}Na cannot be the analogue state of the 3488 keV level in ^{20}F, which is strongly fed in the β-decay of ^{20}O.

For sd-shell nuclei at least three cases of allowed β-transitions (with bound final states) are known, whose log ft values exceed 6, namely ^{17}N, ^{17}Ne and ^{18}N [41]. Therefore, the experimental log ft limit ≥ 6.2 does not completely exclude a J^π-assignment of 1^+. If one assumes the 2645 keV state in ^{20}Na to be the analogue of the 3173 keV, (1^+) state in ^{20}F, a value of $\omega\gamma = 6$ meV is deduced from the known decay properties of the 3173 keV level [6].

Recently a $J^\pi = 3^+$ assignment for the 2645 keV level has been proposed by Brown et al. [8], mainly based on Coulomb shift systematics. In this study, the level was proposed to be the isospin mirror of the 2966 keV, 3^+-state in ^{20}F and a value of 80 meV for $\omega\gamma$ was deduced under this assumption. It was argued that the 2645 keV level in ^{20}Na cannot be the analogue of the 3173 keV state in ^{20}F, since the former is strongly populated in the ^{20}Ne(^{3}He,t)^{20}Na reaction, whereas the latter is only weakly fed in the ^{20}Ne(t,^{3}He)^{20}F reaction. In this context it is interesting to note that an unusually strong population of states close to the break-up threshold has been observed in other cases (see [5] and references therein). Since the 2645 keV level in ^{20}Na is situated close to the proton threshold of ^{20}Na, the strong population of the 2645 keV level in the ^{20}Ne(^{3}He,t)^{20}Na reaction might be explained by such a threshold effect. However, a comparison of the angular distributions for charge-exchange reactions leading to analogue states in ^{20}Na and ^{20}F [42] seems to favour the identification of the 2645 keV level in ^{20}Na as the analogue state to the 2966 keV, 3^+-level in ^{20}F, although the statistics of the compared angular distributions are not particularly convincing. It remains to be clarified whether the threshold effect causing a different population of analogue states could also result in different angular distributions for those analogue states.

4.2. Validity of the Isobaric Mass Multiplet Equation

The isobaric mass multiplet equation [43] (IMME) provides a relation in second order of T_Z between the masses of the $2T + 1$ members of an isobaric multiplet,

$$M(A, T, T_Z) = a(A, T) + b(A, T) \times T_Z + c(A, T) \times T_Z^2, \qquad (4)$$

where A denotes the number of nucleons, T the isospin quantum number and T_Z its projection. Since ^{20}Mg is a $T = 2$ nucleus, the isobaric multiplet consists of five levels, which reside in the nuclei ^{20}O, ^{20}F, ^{20}Ne, ^{20}Na and ^{20}Mg. The properties of those states are given in Table 4. Fig. 9 shows the differences between the experimental results and the least squares fits of second to fourth order polynomials to the masses of the five states,

the additional terms being $d(A,T) \times T_Z^3$ and $e(A,T) \times T_Z^4$. The values for the coefficients a, b, c, d, and e obtained under different conditions imposed on the coefficients d and e, the resulting reduced χ^2_{red}-values and the values obtained for the free coefficients are given in Table 5. As can be seen from Fig. 9, the $T_Z = -2$ residuum for the purely quadratic fit differs by slightly less than one standard deviation from 0. The agreement between the measured masses and the third-order IMME-fit is improved by allowing the coefficient $d(A,T)$ to be $\neq 0$. For purely statistical errors of the measured masses one would expect a scattering of the data around zero, with the scattering being comparable to the size of the error bars. However, this is apparently not the case. Much better agreement between measured masses and fitted values is observed. Our conjecture is either that the good agreement observed is accidental or the size of the experimental uncertainties for low T_Z-values is generally too large. The fit with only $e(A,T)$ forced to be 0 does not give a significant improvement compared to the second order IMME form. We conclude from this discussion that the data available for the A = 20, $T = 2$ multiplet do not yield a strong evidence for a significant deviation from the quadratic IMME-form.

4.3. Isospin Asymmetry in the A = 20 System

From the almost complete charge independence of nuclear forces one expects nearly equal strengths or log ft values for isospin-mirrored β-decays. A deviation from isospin symmetry is expected if one β-decay proceeds to a bound state and its mirror decay to an unbound level. In the A = 20 system the strengths of two allowed $0^+ \rightarrow 1^+$ transitions can be compared, namely

$$(i)\ \ ^{20}\mathrm{O} \rightarrow ^{20}\mathrm{F}\ (E^* = 1057\ \mathrm{keV})\ \text{ and }\ ^{20}\mathrm{Mg} \rightarrow ^{20}\mathrm{Na}\ (E^* = 984\ \mathrm{keV})\ \text{and}$$

$$(ii)\ \ ^{20}\mathrm{O} \rightarrow ^{20}\mathrm{F}\ (E^* = 3488\ \mathrm{keV})\ \text{ and }\ ^{20}\mathrm{Mg} \rightarrow ^{20}\mathrm{Na}\ (E^* = 3001\ \mathrm{keV}).$$

For a comparison between two isospin-mirrored transitions the quantity $\delta = ft^+/ft^- - 1$ is calculated, where $\delta = 0$ denotes perfect isospin symmetry. The ft^+-values for the ^{20}Mg decay were determined from the present experimental data, the ft^--values for the ^{20}O-decay were calculated from the log ft values given in ref. [39] as 3.740 ± 0.006 for case (i) and as 3.65 ± 0.06 for case (ii). For the transitions (i), which proceed to bound states in both nuclei, an asymmetry parameter $\delta = 0.230^{+0.076}_{-0.071}$ calculated. The magnitude of δ agrees with the degree of isospin violation that is expected from other mirror transitions in this mass region. In case (ii), where the ^{20}Mg decay populates a state, that is proton-unbound by 806 keV, an isospin asymmetry parameter $\delta = 1.69^{+0.86}_{-0.65}$ is obtained. This means that B(GT) for the β^--decay is 2.69 times larger than for the β^+-decay. One might argue that the observed isospin asymmetry is caused by the non-observation of part of the transition strength in the case of the ^{20}Mg β-decay, e.g. by a non-observed γ-deexcitation of the proton unbound level at 3001 keV. Indeed, there exists a proton-unbound level in ^{36}K, populated by the β^+-decay of ^{37}Ca, whose γ-width exceeds its proton-width by far [44], so that a too high value for ft^+ is determined if one relies on proton data alone. However, in our case the asymmetry cannot be fully explained by a γ-deexcitation of the

3001 keV level, since γ-rays due to the radiative decay of this level have not been observed (see Sect. 3.3).

This asymmetry is the largest one observed so far for unbound states, as can be seen from a comparison with the compilation in ref. [45]. It may be speculated that the asymmetry is related to an unusually extended proton wave function of the 3001 keV state in ^{20}Na. However, up to now no satisfying theoretical explanation for the asymmetry has been found. A clarification would be desirable since the assumption of isospin symmetry in systems involving unbound states plays a role e.g. for the calibration of the ^{37}Cl solar neutrino detector [46] by the investigation of the ^{37}Ca βp-decay.

4.4. Comparison with Shell-Model Calculations

The β-decay of ^{20}Mg and the subsequent proton decay of states in ^{20}Na to positive parity states in ^{19}Ne have been calculated within the sd-shell model space following the methods outlined in [47] and [48]. The theoretical ^{20}Mg half-life of 101.8 ms, calculated with the effective operator of ref. [47], agrees very well with the value of 95 $\pm$ 3 ms as obtained in this experiment. Although the effective operator of ref. [47] is state dependent, to within a few-percent it is equivalent to an overall hindrance factor of $1/0.6 = 1.67$. The absolute value and the distribution of the GT-strength of the ^{20}Mg β-decay will be discussed in Sect. 4.5. For all particle-unbound ^{20}Na states the calculated proton emission is dominated by s-wave decay to the $1/2^+$-ground state of ^{19}Ne. The calculated branching to the lowest $5/2^+$- and $3/2^+$-levels at 238 and 1536 keV excitation energy relative to the ground state branching amounts to 0.13 and 0.01. This has to be compared to the experimentally determined values of 0.10 and 0.06. The agreement with the experiment is good for the $5/2^+$-state but only moderate for the $3/2^+$-level. The total calculated widths of the ^{20}Na levels range from 0.3 keV for the isospin-forbidden decay of the IAS to about 2 MeV for the isospin-allowed decay of the 6th theoretical 1^+-state which lies near the IAS and has the largest B(GT) value. There are indications for such a broad state in the data, but due to its width and the $\beta\alpha$ background events present in the particle spectra it is not possible to extract a branching ratio for this broad level.

4.5. The Quenching of the Gamow-Teller Strength

There is evidence that the measured GT strength is generally lower than that calculated within the framework of a nuclear shell model, cf. e.g. [47]. This situation is referred to as the quenching of the GT strength. In order to investigate this effect, a total strength

$$T(GT) = \frac{1}{W}[\sum B(GT)]^{1/2} \qquad (5)$$

is defined. The sum extends over all levels in the daughter nucleus. W is a weighting factor which normalizes $T(GT)$ to 1 for a decay that fully exhausts the sum-rule limit:

$$W = \frac{g_A}{g_V}[(2J_i + 1) \times 3(Z_i - N_i)]^{1/2}. \tag{6}$$

g_V and g_A are the vector- and axial-vector coupling constants, and J_i, Z_i and N_i denote the spin, atomic number and neutron number of the decaying nucleus.

^{20}Mg is a favourable candidate for the investigation of the quenching of the GT strength, since the shell model calculation introduced in Sect. 4.4 predicts as much as 79% of the GT-strength to reside within the Q_{EC} window. The experimental strength distribution for the decay of ^{20}Mg was determined by using the Q_{EC}-value of the ^{20}Mg-β-decay (10726 $\pm$ 28 keV) and the proton separation energy of ^{20}Na (2195 $\pm$ 7 keV), both taken from ref. [25], the value of 95 $\pm$ 3 ms for the ^{20}Mg half-life (see Sect. 3.3), the ^{20}Na level energies and the β-decay branching ratios b_β given in Table 3. Electron capture processes were neglected and the Fermi integral $f_{\beta+}$ for nuclear β^+-decay was taken from ref. [49]. Using the relation

$$B(GT) = \frac{6177[\mathrm{s}]}{(\mathrm{g_A/g_V})^2 \times \mathrm{T_{1/2}} \times \mathrm{b_\beta} \times \mathrm{f_{\beta+}}}, \tag{7}$$

$B(GT)$ was calculated for each individual transition. The respective ^{20}Na level energies, β-decay branching ratios, the resulting log ft values and $B(GT)$-values as well as the deduced J^π-assignments are given in Table 6.

The $T(GT)$ values were determined for the experimental and calculated $B(GT)$-values according to eq. (5). The sum in eq. (5) was restricted to transitions which populate levels below the IAS. The resulting quenching factor of the GT-strength amounts to

$$\frac{T(GT)_{exp.}}{T(GT)_{calc.}} = 0.84 \pm 0.18$$

This value was obtained by employing the B(GT) values of 0.45 and 0.79 for the broad levels at 4800 and 5600 keV, respectively. If the lower B(GT) limits of 0.23 and 0.42 are used for the respective states, a quenching factor of 0.77 is obtained. Globally, for the sd shell data about 60% (0.77 $\times$ 0.77) of the predicted strength is observed in β-decay and in charge-exchange reactions. Our observation of 71% (0.84 $\times$ 0.84) of the predicted GT strength (below the IAS) is in fair agreement with the global value.

Besides this global comparison it is interesting to discuss the measured and experimental strength distributions in more detail as a function of the ^{20}Na excitation energy. Fig. 10 shows the calculated Fermi- and GT-strength distribution in comparison to the experimental data from this work. The Fermi strength for the ^{20}Mg decay to the IAS at 6533 keV in ^{20}Na should be exactly four, which is in agreement with the experimentally determined value 4.57 $\pm$ 0.68. Below a ^{20}Na excitation energy of 3 MeV both in the calculation and in the experiment one state is seen with good agreement obtained for the excitation energy and fair agreement obtained for the GT-strength. The theoretical level predicted at 3.3

MeV seems to be fragmented over at least three states with excitation energies between approximately 3 and 4 MeV. This might be seen as an indication of nuclear deformation which causes different Nilsson orbitals to split up in energy. The shell model calculation predicts the GT giant resonance to lie between 4.8 and 7.2 MeV. The comparison with the experimental data is difficult in this energy region as the states populated are numerous and may also be broad. Correspondingly, the identification of single levels is difficult. Only two groups of levels around 4.8 and 5.6 MeV were identified. For levels above the IAS, only lower limits for B(GT) can be given, which have been deduced from the observed proton emission to excited states in ^{19}Ne. No GT strength was measured for excitation energies above 7.4 MeV.

5. Summary and Outlook

The experiment described in this article has demonstrated the possibility to use sources of short-lived nuclei, produced by intermediate-energy fragmentation reactions, for detailed β-decay studies. It is worth noting that, according to the estimated proton separation energy of 660 $\pm$ 500 keV of ^{19}Mg [25], ^{20}Mg may well represent the lightest bound magnesium isotope. β-delayed particle-, γ-ray-, and particle-γ-coincidence spectra have been obtained. The experimental data allowed us to determine for the first time a detailed partial decay scheme of ^{20}Mg which includes several new states in ^{20}Na and their deexcitation properties. The question of the quenching of the GT-strength and of the isospin symmetry have been investigated for this exotic nucleus. Although this experiment gives the most stringent limit obtained so far for the log ft value of the astrophysically interesting 2645 keV state in ^{20}Na, no definite conclusion can yet be drawn concerning its spin and parity.

One possibility of further investigating the properties of the 2645 keV level in ^{20}Na and the β-decay of ^{20}Mg would be an experimental set-up at LISE3 optimized for the detection of low-energy protons. It could be realized by using a stack of very thin and possibly segmented silicon detectors for the implantation of ^{20}Mg and the spectroscopy of the subsequent proton decay. With such a detector stack the background due to the energy deposition of β-rays in the implantation detectors could be considerably reduced and it should be possible to achieve a lower limit for the log ft value of the 2645 keV state of ^{20}Na between 7 and 8. This limit would almost definitely exclude a J^π-assignment of 1^+ for this state.

If the spin and parity of the 2645 keV level is 3^+ as suggested by Brown et al. [8], the corresponding log ft value would be approximately 12, so that a population of the level with beam intensities available at the LISE3 spectrometer becomes impossible. Instead, an isotope separator on-line (ISOL) experiment with a chemically selective ion-source could be performed. If such an experiment yielded an isotopically clean ^{20}Mg beam of sufficient strength, the detection of the exceedingly small β-branching ratio of 10^{-9}, corresponding to a log ft value of 12, might become possible. Furthermore, the production of point-like thin

sources by means of the ISOL method would make it possible to use a telescope detector for the idenfication of β-delayed protons and greatly reduce the β- and $\beta\alpha$-background.

Recently, Hofstee et al., who reinvestigated the (^{3}He,t) reaction, reported indications of γ-rays from the deexcitation of the 2645 keV state in ^{20}Na [50]. It seems to be possible that the ratio of the γ-to-proton width for the 2645 keV level can be determined from those experimental data.

Another very promising attempt to clarify the properties of the ^{19}Ne$(p,\gamma)^{20}$Na reaction is being made at the ARENAS3 facility at Leuven. The astrophysically interesting ^{19}Ne(p,γ) reaction is simulated by using a radioactive ^{19}Ne beam impinging onto a polyethylene target in an inverse-kinematics experiment [51,52].

One of us (BAB) would like to acknowledge support from the Humboldt Foundation and NFS Grant 90-17077.

References

[1] R. K. Wallace and S. E. Woosley, Astrophys. J. Suppl. 45 (1981) 389

[2] P. V. Magnus, M. S. Smith, A. J. Howard, P. D. Parker and A. E. Champagne, Nucl. Phys. A506 (1990) 332

[3] S. Kubono, N. Ikeda, M. Yasue, T. Nomura, Y. Fuchi, H. Kawashima, S. Kato, H. Orihara, T. Shinozuka, H. Ohnuma, H. Miyatake and T. Shimoda, Z. Phys. A331 (1988) 359

[4] S. Kubono, H. Orihara, S. Kato and T. Kajino, Astrophys. J. 344 (1989) 460

[5] N. M. Clarke, P. R. Hayes, M. B. Becha, C. N. Pinder and S. Roman, Nucl. Part. Phys. 16 (1990) 1547

[6] L. O. Lamm, C. P. Browne, J. Görres, S. M. Graff and M. Wiescher, Nucl. Phys. A510 (1990) 503

[7] M. S. Smith, P. V. Magnus, K. I. Hahn, A. J. Howard, P. D. Parker, A. E. Champagne and Z. Q. Mao, Nucl. Phys. A536 (1992) 333

[8] B. A. Brown, A. E. Champagne, H. T. Fortune and R. Sherr, Phys. Rev. C48 (1993) 1456

[9] D. M. Moltz, M. D. Cable, R. D. von Dincklage, R. F. Parry, J. M. Wouters and J. Cerny, Phys. Rev. Lett. 42 (1979) 43

[10] J. Äystö, M. D. Cable, R. F. Parry, J. M. Wouters, D. M. Moltz, and J. Cerny, Phys. Rev. C23 (1981) 879

[11] S. Kubono, N. Ikeda, Y. Funatsu, M. H. Tanaka, T. Nomura, H. Orihara, S. Kato, M. Ohura, T. Kubo, N. Inabe, A. Yoshida, T. Ichihara, M. Ishihara, I. Tanihata, H. Okuno, T. Nakamura, S. Shimoura, H. Toyokawa, C. C. Yun, H. Ohnuma, K. Asahi, A. Chakraberti, T. Mukhopadhyay and T. Kajino, Phys. Rev. C46 (1992) 361

[12] J. Görres, M. Wiescher, K. Scheller, D. J. Morrissey, B. M. Sherrill, D. Bazin and J. A. Winger, Phys. Rev. C46 (1992) R833

[13] A. Piechaczek, M. F. Mohar, R. Anne, V. Borrel, J. M. Corre, D. Guillemaud-Mueller, M. Ishihara, H. Keller, S. Kubono, V. Kunze, M. Lewitowicz, P. Magnus, A. C. Mueller, T. Nakamura, M. Pfützner, E. Roeckl, K. Rykaczewski, M. G. Saint-Laurent, W.-D. Schmidt-Ott, O. Sorlin, Proc. 6th Int. Conf. on Nuclei Far From Stability & 9th Int. Conf. on Atomic Masses and Fundamental Constants, Bernkastel-Kues, 1992; R. Neugart and A. Wöhr (eds.), Inst. Phys. Conf. Ser. No. 132; Section 7 (1993), p. 851

[14] A. Piechaczek, M. F. Mohar, R. Anne, V. Borrel, B. A. Brown, J. M. Corre, D. Guillemaud-Mueller, R. Hue, M. Ishihara, H. Keller, S. Kubono, V. Kunze, M. Lewitowicz, P. Magnus, A. C. Mueller, T. Nakamura, M. Pfützner, E. Roeckl, K. Rykaczewski, M. G. Saint-Laurent, W.-D. Schmidt-Ott, O. Sorlin, Proc. 3rd Int. Conf. on Radioactive Nuclear Beams, East Lansing, May 1993, D. J. Morrisey (ed.), Editions Frontieres, 1993, p. 495

[15] A. Piechaczek, M. F. Mohar, R. Anne, V. Borrel, B. A. Brown, J. M. Corre, D. Guillemaud-Mueller, R. Hue, M. Ishihara, H. Keller, S. Kubono, V. Kunze, M. Lewitowicz, P. Magnus, A. C. Mueller, T. Nakamura, M. Pfützner, E. Roeckl, K. Rykaczewski, M. G. Saint-Laurent, W.-D. Schmidt-Ott, O. Sorlin, Proc. Gran Sasso Conference on Nuclear Astrophysics, Gran Sasso, Italy, July 1994, to be published

[16] R. Anne, D. Bazin, A. C. Mueller, J. C. Jacmart and M. Langevin, Nucl. Instr. and Meth. A257 (1987) 215

[17] A. C. Mueller and R. Anne, Nucl. Instr. and Meth. B56/57 (1991) 559

[18] R. Anne and A. C. Mueller, Nucl. Instr. and Meth. B70 (1992) 276

[19] V. Borrel, B. Gatty, D. Guerreau, J. Galin and D. Jacquet, Z. Phys. A324 (1986) 205

[20] K. Sümmerer, W. Brüchle, D. J. Morrissey, M. Schädel, B. Szweryn and Y. Weifan, Phys. Rev. C42 (1990) 2546

[21] K. Sümmerer, private communication 1992

[22] J. P. Dufour, R. Del Moral, H. Emmermann, F. Hubert, D. Jean, C. Poinot, M. S. Pravikoff and A. Fleury, Nucl. Instr. and Meth. A248 (1986) 267

[23] D. F. Torgerson, K. Wien, Y. Fares, N. S. Oakey, R. D. Macfarlane and W. A. Lanford, Phys. Rev. C8 (1973) 161

[24] E. T. H. Clifford, E. Hagberg, J. C. Hardy, H. Schmeing, R. E. Azuma, H. C. Evans, V. T. Koslowsky, U. J. Schrewe, K. S. Sharma and I. S. Towner, Nucl. Phys. A493 (1989) 293

[25] G. Audi and A. H. Wapstra, Nucl. Phys. A565 (1993) 1

[26] GEANT User's Guide, M. Maire, CERN, Revised Version 06.01.92

[27] D. Bazin, O. Sorlin, LISE computer code, private communication, 1993

[28] J. Lindhard, V. Nielsen, M. Scharff and P. V. Thomsen, Mat. Fys. Medd. Dan. Vid. Selsk 33, no. 10 (1963) 1

[29] J. Lindhard, M. Scharff and H. E. Schiøtt Mat. Fys. Medd. Dan. Vid. Selsk 33, no. 14 (1963) 1

[30] B. D. Wilkins, M. J. Fluss, S. B. Kaufman, C. E. Gross and E. P. Steinberg, Nucl. Instr. Meth. 92 (1971) 381

[31] C. Chasman, K. W. Jones and R. A. Ristinen, Phys. Rev. Lett. 15 (1965) 245; C. Chasman, K. W. Jones, R. A. Ristinen and J. T. Sample, Phys. Rev. 154 (1967) 239

[32] A. R. Sattler, Phys. Rev. 138 (1965) A1815

[33] E. L. Haines and A. B. Whitehead, Rev. Sci. Instr. 37 (1966) 190

[34] T. Karcher and N. Wotherspoon, Nucl. Instr. Meth. 93 (1971) 519

[35] R. D. Campbell and R. P. Lin, Rev. Sci. Instr. 44 (1973) 1510

[36] J. J. Grob, A. Grob, A. Pape and P. Siffert, Phys. Rev. B11 (1975) 3273

[37] A. Grob, J. J. Grob and P. Siffert, Nucl. Instr. Meth. 132 (1976) 273

[38] P. Hungerford, T. von Egidy, H. H. Schmidt, S. A. Kerr, H. G. Börner, and E. Monnand, Z. Phys. A 313 (1983) 339

[39] D. E. Alburger, G. Wang and E. K. Warburton, Phys. Rev. C35 (1987) 1479

[40] E. K. Warburton and B. A. Brown, Phys. Rev. C46 (1992) 923

[41] W. T. Chou, E. K. Warburton and B. A. Brown, Phys. Rev. C47 (1993) 163

[42] N. M. Clarke, S. Roman, C. N. Pinder and P. R. Hayes, J. Phys. G19 (1993) 1411

[43] E. P. Wigner, Proceedings of the Robert A. Welch Conferences on Chemical Research, Robert A. Welch Foundation, Houston, Texas 1957, Vol. 1, p. 67

[44] W. Trinder, Doktorarbeit, Universität Frankfurt a. M., in preparation

[45] M. J. G. Borge, J. Deding, P. G. Hansen, B. Jonson, G. Martinez Pinedo, P. Møller, A. Richter, K. Riisager and O. Tengblad, Phys. Lett. B 317 (1993) 25

[46] R. Davis, A. K. Mann and L. Wolfenstein, Annu. Rev. Nucl. Part. Sci. 39 (1989) 467

[47] B. A. Brown and B. H. Wildenthal, At. Data and Nucl. Data Tables 33 (1985) 347

[48] B. A. Brown, Phys. Rev. Lett. 65 (1990) 2753

[49] B. S. Dzhelepov, L. N. Zyrianova, Y. P. Suslov, Beta-processes – Functions for Analysis of Beta-spectra and Electron-capture, Nauka, Leningrad 1972

[50] M. Hofstee et al., Proc. 3rd Int. Symp. on Nuclear Astrophysics Nuclei in The Cosmos, Gran Sasso, Italy, July 1994, to be published

[51] R. Coszach et al., Proc. 2nd Int. Symp. on Nuclear Astrophysics Nuclei in The Cosmos, Karlsruhe 1992, F. Käppeler and K. Wisshak (eds.), IOP Publishing Ltd, 1993, p. 295

[52] R. D. Page, A. C. Shotter, C. R. Brain, F. Binon, R. Coszach, T. Davinson, T. Delbar, P. Decrock, P. Duhamel, W. Galster, M. Huyse, P. Leleux, I. Licot, E. Lienard, P. Lipnik, C. Michotte, A. Ninane, P. J. Sellin, G. Vancraeynest, P. Van Duppen, J. Vanhorenbeek, J. Vervier and P. J. Woods, Proc. 3rd Int. Conf. on Radioactive Nuclear Beams, East Lansing, USA, May 1993

Table 1
The released energies and the origin of the proton lines observed in this experiment.

	released energy [keV]	^{20}Na-level → ^{19}Ne-level
p_1	806(2)	3001 → 0
p_2	1056	4800 → 1536
p_3	1441	3874 → 238 ?
p_4	1679(15)	3874 → 0
p_5	1928(16)	4123 → 0
p_6	2344	4800 → 238, 275
p_7	2559	4800 → 0 ?
p_8	2884	?
p_9	3837	6266 → 238, 275
p_{10}	4071(30)	6266 → 0, 6521 → 238, 275
p_{11}	4326(30)	6521 → 0

Table 2
The β-decay of ^{20}Mg and the subsequent γ- and proton-decay into levels in ^{20}Na and ^{19}Ne. The ^{19}Ne levels populated are indicated by their J^π-values and excitation energies. All branching ratios refer to the number of implanted ^{20}Mg atoms as 100%, the error amounts to 12% of the given value unless otherwise indicated. Two groups of unresolved levels are marked by an asterisk. For those level groups the individual ^{20}Na excitation energy ranges [MeV] are given behind the branching ratios. a) sum of feeding amounts to ≈ 3%, those 3% branching are not included into the summed intensities of the last line.

$E^{exc.}_{^{20}Na}[keV]$	b_β[%]	$1/2^+$, g.s	$5/2^+$, 238 keV	$1/2^-$, 275 keV	$5/2^-$, 1508 keV	$3/2^+$, 1536 keV
984.25(0.10)	69.7(1.2)	÷	÷	÷	÷	÷
2645	< 0.1	<0.1	÷	÷	÷	÷
3001(2)	11.5	11.5	÷	÷	÷	÷
3874(15)	4.8	4.8	÷	÷	÷	÷
4123(16)	2.7	1.1	0.4	1.2	÷	÷
≈ 4800 *)	>1.9	a)	0.3 [4.5-5.0]	0.8 [4.6-5.1]	0.1 [4.9-5.8]	0.7 [4.7-5.2]
≈ 5600 *)	> 1.5	a)	0.8 [5.4-6.2]	0.7 [5.2-6.0]	0.04 [5.8-5.9]	÷
6266(30)	1.2	0.7	0.2	0.1	0.04 [6.0-6.3]	0.1
6521(30)	3.3	1.8	0.59	0.32	0.07	0.51
≈ 6770	>0.03	÷	0.03	÷	÷	÷
≈ 6920	>0.01	÷	0.01	÷	÷	0.02
≈ 7440	>0.01	÷	÷	÷	÷	0.01
$\sum$	96.7	> 19.9	2.3	3.1	0.25	1.3

Table 3

Compilation of ^{20}Na levels as observed in this experiment and other experiments. Given are the excitation energies of ^{20}Na levels in keV and J^{π}-assignments. The last column contains the weighted mean value of the energy and the J^{π}-assignment which is compatible with all experimental values. The adopted value of the IAS excitation energy of 6534 keV was calculated including the value of 6574 ± 50 keV from ref. [9].

This work	[11]	[12]	[4]	[3] [4]	[5]	[6]	[7]	[50]	adopted value
βp	βp	βp	p,n	^{3}He,t	^{3}He,t	^{3}He,t	^{3}He,t	$p\gamma$	
			580(15) 3+	600(15) (345)+	595(20) 3+	606(13) 3+			596(8) 3+
			790(15) 4+	802(15) (345)+	801(20) 4+	808(11) 4+			802(7) 4+
984.25(0.10) 1+			993(15) 1+	990(15) (123)+	996(20) (1+−)	996(12) 1+			984.25(10) 1+
			1353(15) (2−)	1347(15) (234)−	1350(20) 2−	1338(14) 2−			1346(8) 2−
			1843(15) (2−)	1832(15) (234)−	1819(20) 2−	1841(11) 2+−			1837(7) 2−
			2016(20) (3−)	1967(20) (234)−	1992(20) (3+−2−)	1993(12) 3−	1990		1992(8) 3−
				2034(20) (345)+	2100(40) (345+−)	2064(16) (23)+	2060		2057(12) 3+
			2651(20) 1+	2637(15) (01)+	2640(20) (1+−)	2649(16) 1+	2646(9)		2645(6) 1+?
			2852(20) (23)+	2842(15) (345)+	2860(20) (3,4+−)	2836(12) 3+	2857(9)		2849(6) 3+
				2967(20)	3010(20) > 3−, > 4+	2972(13)	2986(9)		2983(7) > 3−, > 4+
3001(2)* 1+	3046	3006(10) 1+						3001(2) (1+)	3001(2) 1+
			3053(20)	3046(20) (123)+			3056(9)	3068(2) (0+)	3067(2)
				3302(30) (456)−	3290(20) (234+−)	3324(11) (12)+			3315(9)
			3636(20)	3644(30) ((234)−)	3690(60) (23−4+−)				3642(16) (234)−
3874(15) 1+	3868 1+		3869(11) 1+	3840					3871(9) 1+
4123(16) 1+	4090 1+								4123(16) 1+
				4160	4150(60) (4−+2−)				4150(60) (4−+2−)
				4620	4560(60) (2+−)				4560(60) (2+−)
≈ 4800 1+									≈ 4800 1+
					5170(60)				5170(60)
≈ 5600 1+					5430(60)				≈ 5600 1+
6266(30) 1+									6266(30) 1+
6521(30) 0+	6440 0+	6533(15) 0+							6534(13) 0+

Table 4
Compilation of the lowest lying T = 2 levels in the A = 20 nuclei. Given are the isospin projection quantum number T_Z, the nucleus which contains the level, the ground-state mass excess, the excitation energies of the levels and their total decay widths.

T_Z	Nuclide	Mass excess [keV]	E^* [keV]	Γ_{total} [keV]
-2	^{20}Mg	17571(27)	0	
-1	^{20}Na	6845(7)	6534(13)	
0	^{20}Ne	-7041.929(0.003)	16732(5)	2.0(5) (γ, p, α)
1	^{20}F	-17.40(0.08)	6519(3)	
2	^{20}O	3796.9(1.2)	0	

Table 5
Polynomial coefficients a, b, c, d, and e (first line) and their errors (second line) as obtained from polynomial fits to the experimental masses of the A = 20, T = 2 multiplet under different restrictions for the coefficients, indicated by $\equiv 0$. Additionally, the reduced χ^2_{red}-values and the resulting probabilities p are given.

a [MeV]	b [MeV]	c [MeV]	d [MeV]	e [MeV]	χ^2_{red}	p[%]
9.6937	-3.4393	0.2455	$\equiv 0$	$\equiv 0$	1.252	53
0.0035	0.0046	0.0021				
9.6905	-3.4354	0.2486	-0.0021	$\equiv 0$	0.037	85
0.0046	0.0058	0.0035	0.0019			
9.6901	-3.4414	0.2545	$\equiv 0$	-0.0018	0.223	64
0.0050	0.0051	0.0091		0.0017		
9.6901	-3.4371	0.2508	-0.0016	-0.0006	÷	÷
0.0050	0.0010	0.0012	0.0034	0.0003		

Table 6
Properties of ^{20}Na levels as observed in this experiment. Given are the excitation energy, the β-decay branching ratio, the log ft value, the B(GT) value and and the J^π-assignment. The asterisk symbol indicates broad or unresolved states, for which b_β could be determined only from proton emission to excited ^{19}Ne levels. For those states the numbers in square brackets indicate the estimated b_β-, log ft-, and B(GT) values under inclusion of the 3% branching to the ^{19}Ne groundstate which is indicated by a) in Table 2.

$E^{exc.}_{^{20}Na}$ [keV]	b_β [%]	log ft	B(GT)	J^π
984.25(0.10)	69.7(1.2)	3.83(2)	0.579(30)	1^+
2645	$\leq$ 0.1	$\geq$ 6.24	$\leq$ 0.002	?
3001(2)	11.5(1.4)	4.08(6)	0.33(5)	1^+
3874(15)	4.8(6)	4.17(6)	0.27(4)	1^+
4123(16)	2.7(3)	4.33(6)	0.18(3)	1^+
4800*	$\geq$1.9 [3.6(0.5)]	$\leq$ 4.23 [3.95(6)]	$\geq$ 0.23 [0.45(7)]	1^+
5600*	$\geq$1.5 [2.8(0.4)]	$\leq$ 3.97 [3.70(6)]	$\geq$ 0.42 [0.79(10)]	1^+
6266(30)	1.2(1)	3.72(6)	0.75(11)	1^+
6521(30)	3.3(4)	3.13(6)	B(F) 4.57(68)	0^+
6770(100)	$\geq$0.03	$\leq$ 5.01	$\geq$ 0.04	(1^+)
6920(100)	$\geq$0.01	$\leq$ 5.39	$\geq$ 0.03	(1^+)
7440(100)	$\geq$0.01	$\leq$ 4.99	$\geq$ 0.04	(1^+)

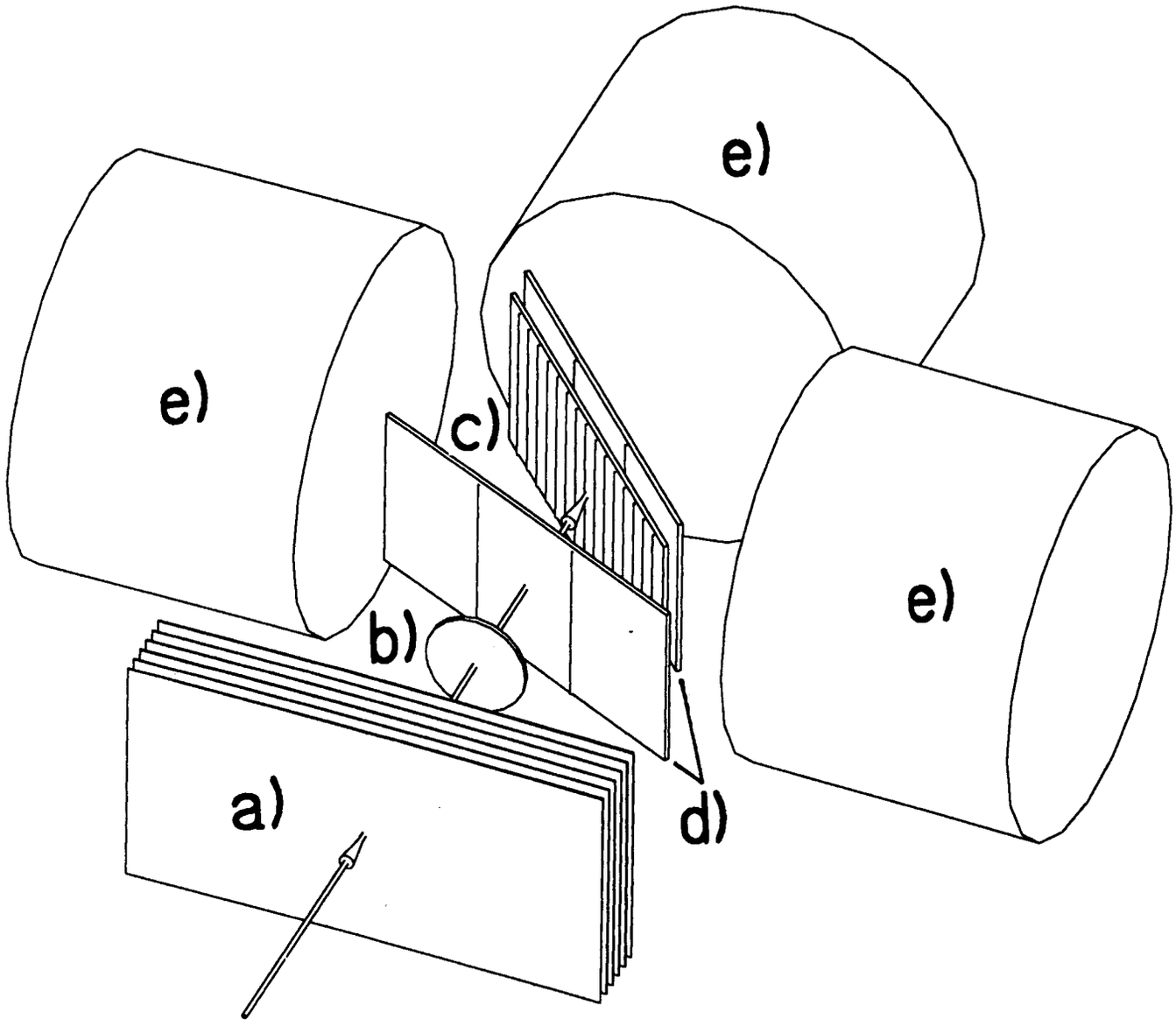

Fig. 1. Detector array for ion implantation and decay spectroscopy; a) stack of foil degraders, b) energy-loss detector, c) implantation detector, d) β-detectors, e) germanium γ-dectectors.

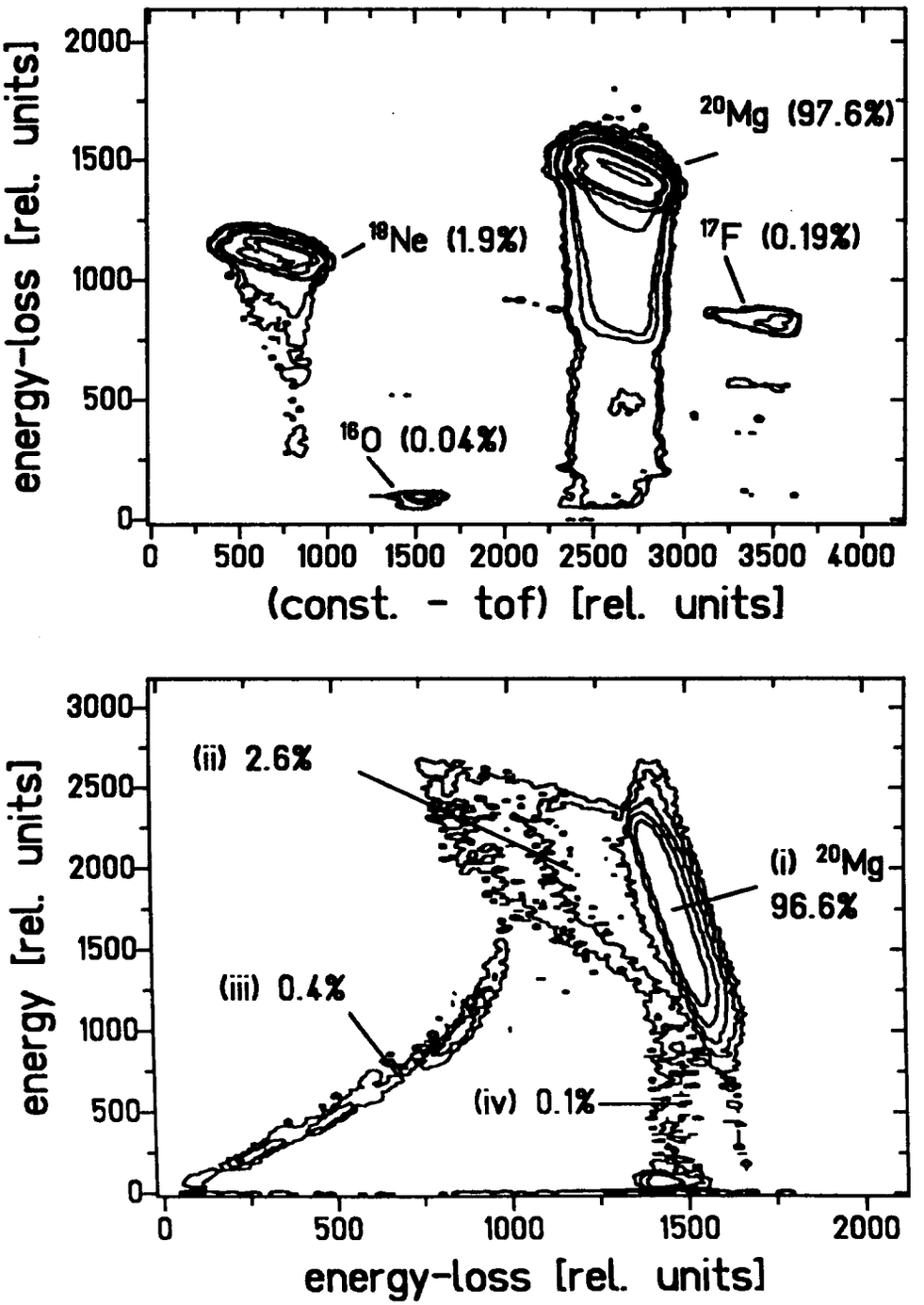

Fig. 2. Energy-loss vs. time-of-flight spectrum (upper part) and energy vs. energy-loss spectrum (lower part). The abundances of ^{20}Mg and the main contaminants are indicated in the upper part. The energy vs. energy-loss spectrum was accumulated under the condition that the registered event was identified as ^{20}Mg in the energy-loss vs. time-of-flight spectrum. In the lower part, the abundance of ^{20}Mg is indicated as well as abundances of different classes of secondary reactions (see text).

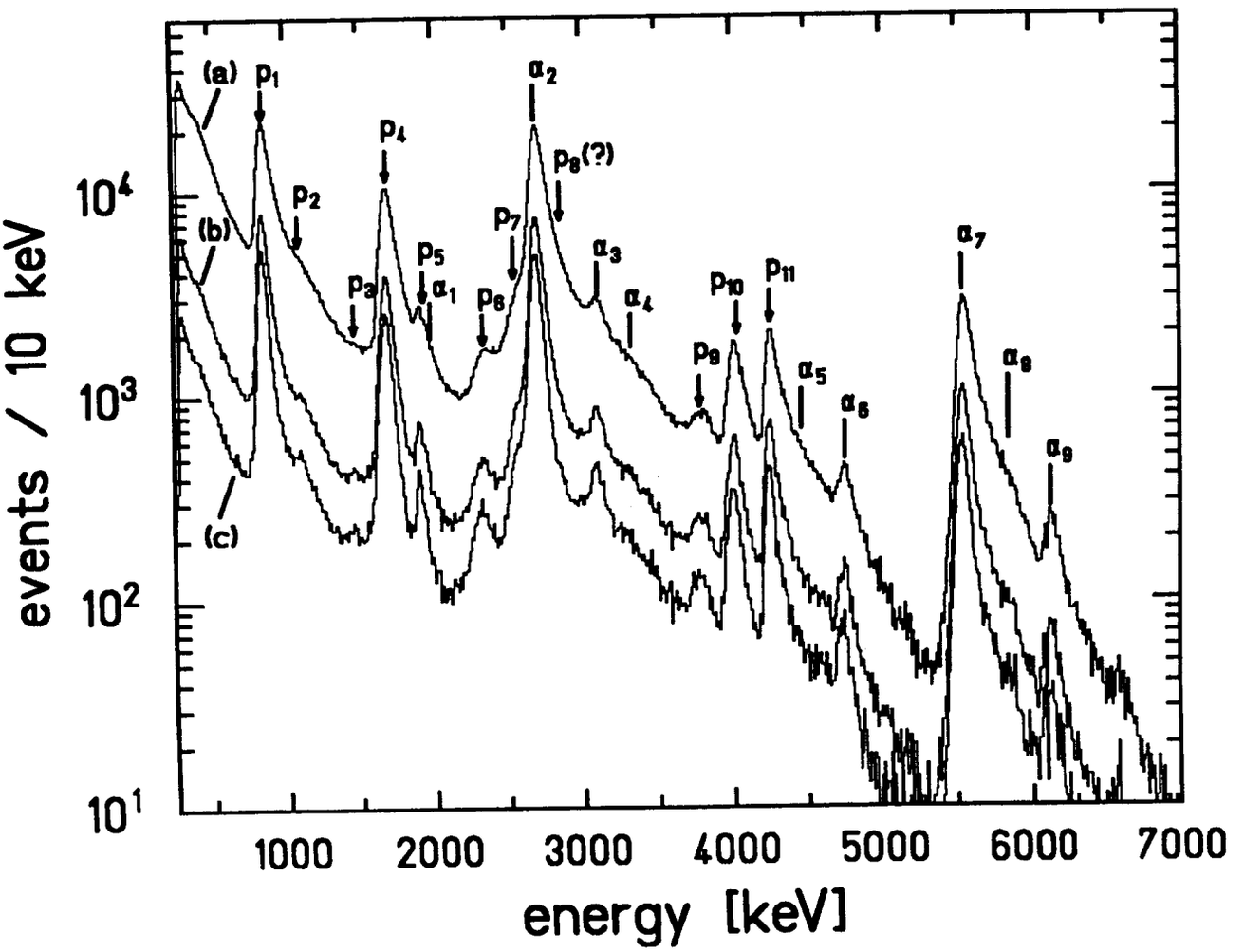

Fig. 3. Spectra of decay events in the six central strips of the implantation detector, recorded under different coincidence conditions with the β-counters (see text). Lines stemming from the βp-decay of ^{20}Mg are marked by p_1 to p_{11}, lines from the $\beta\alpha$-decay of ^{20}Na by α-symbols. The abscissa represents the total energy deposited in the implantation detector, calibrated approximately by using the $\beta\alpha$-lines α_2 and α_7 from the ^{20}Na decay.

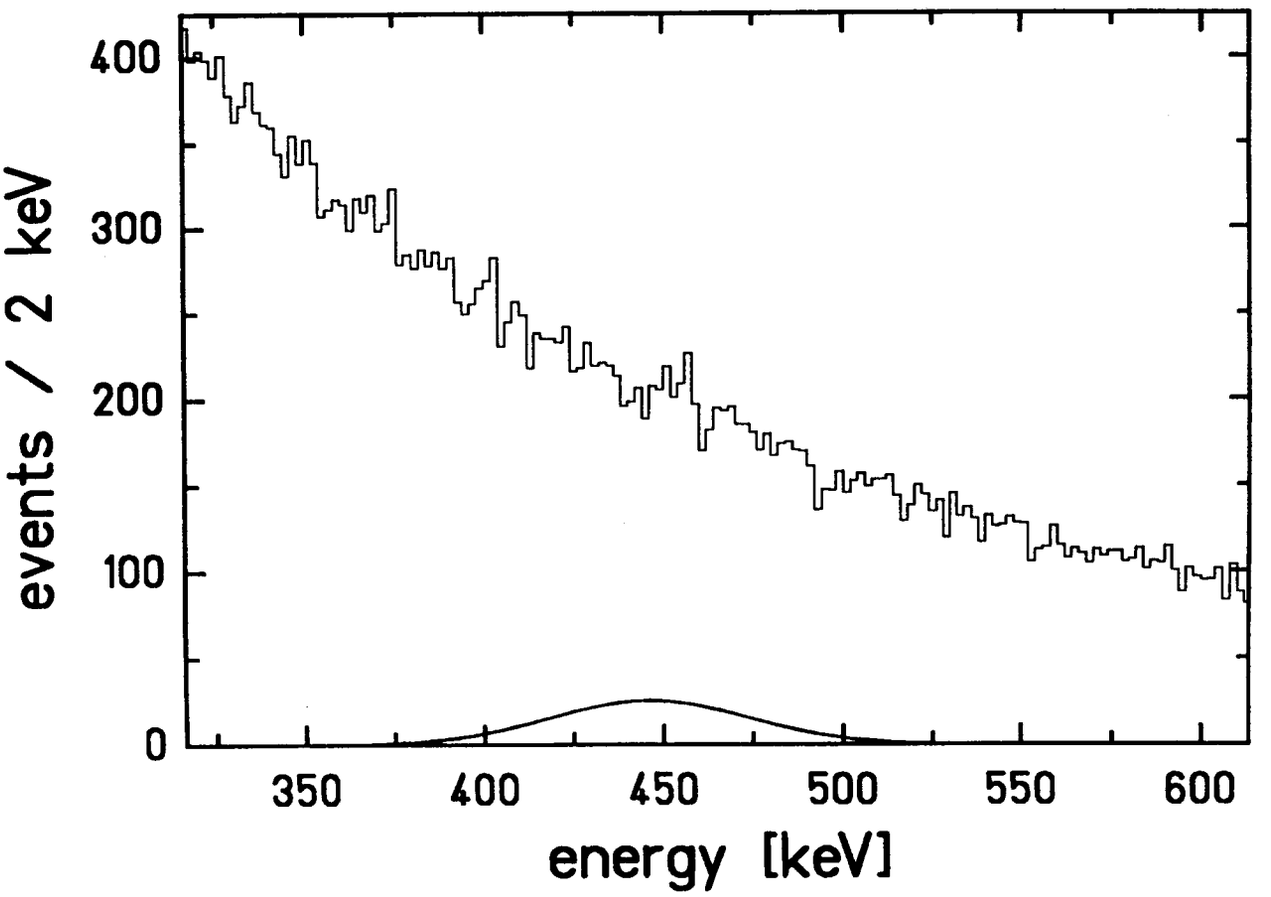

Fig. 4. Low-energy part of the decay spectra in the implantation detector. The expected proton line from the decay of the 2645 keV level in ^{20}Na with an intensity of 0.1% is indicated.

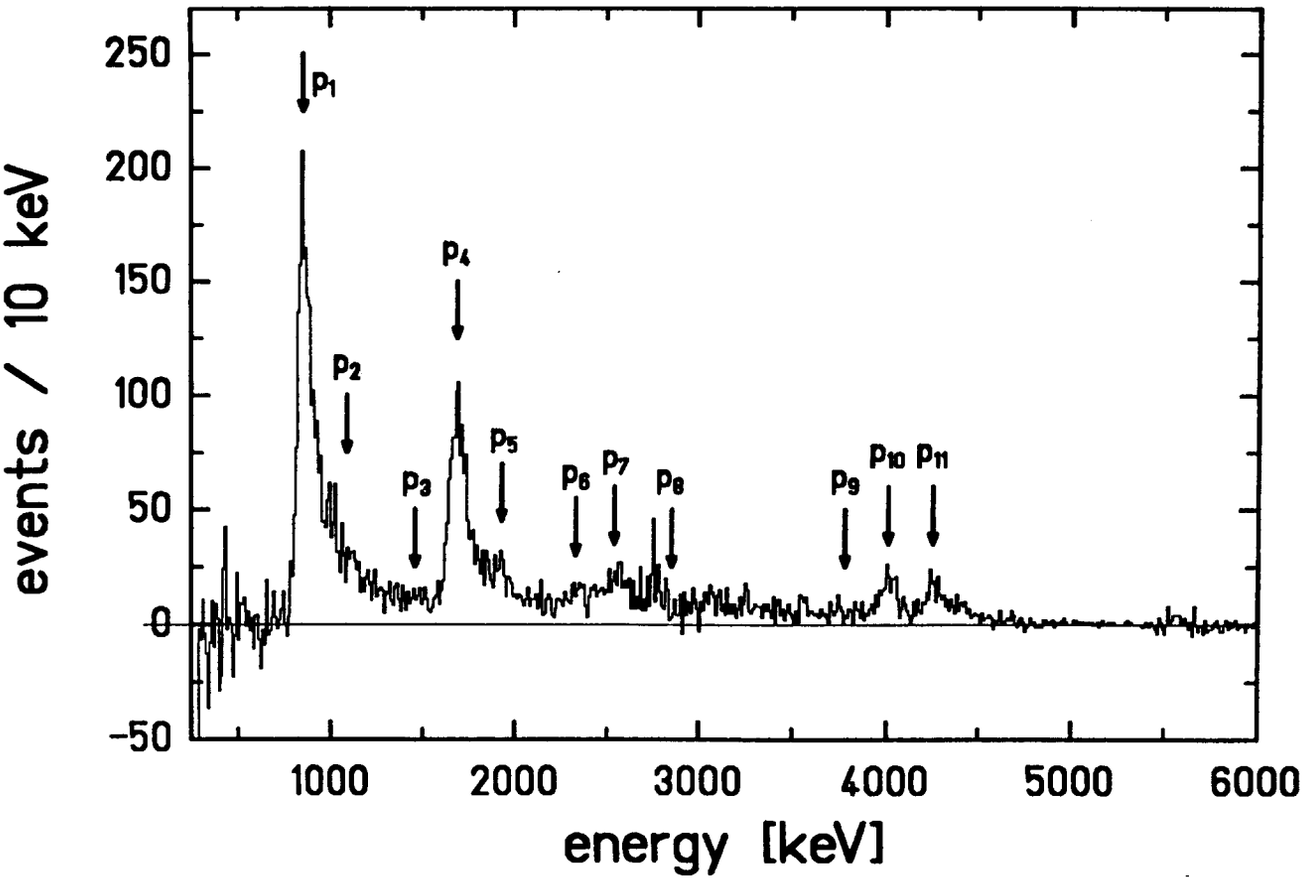

Fig. 5. Energy spectrum of the βp-activity from the decay of ^{20}Mg, recorded in the pulsed-beam mode. The arrows indicate the positions of the lines stemming from the βp-spectrum displayed in Fig. 3.

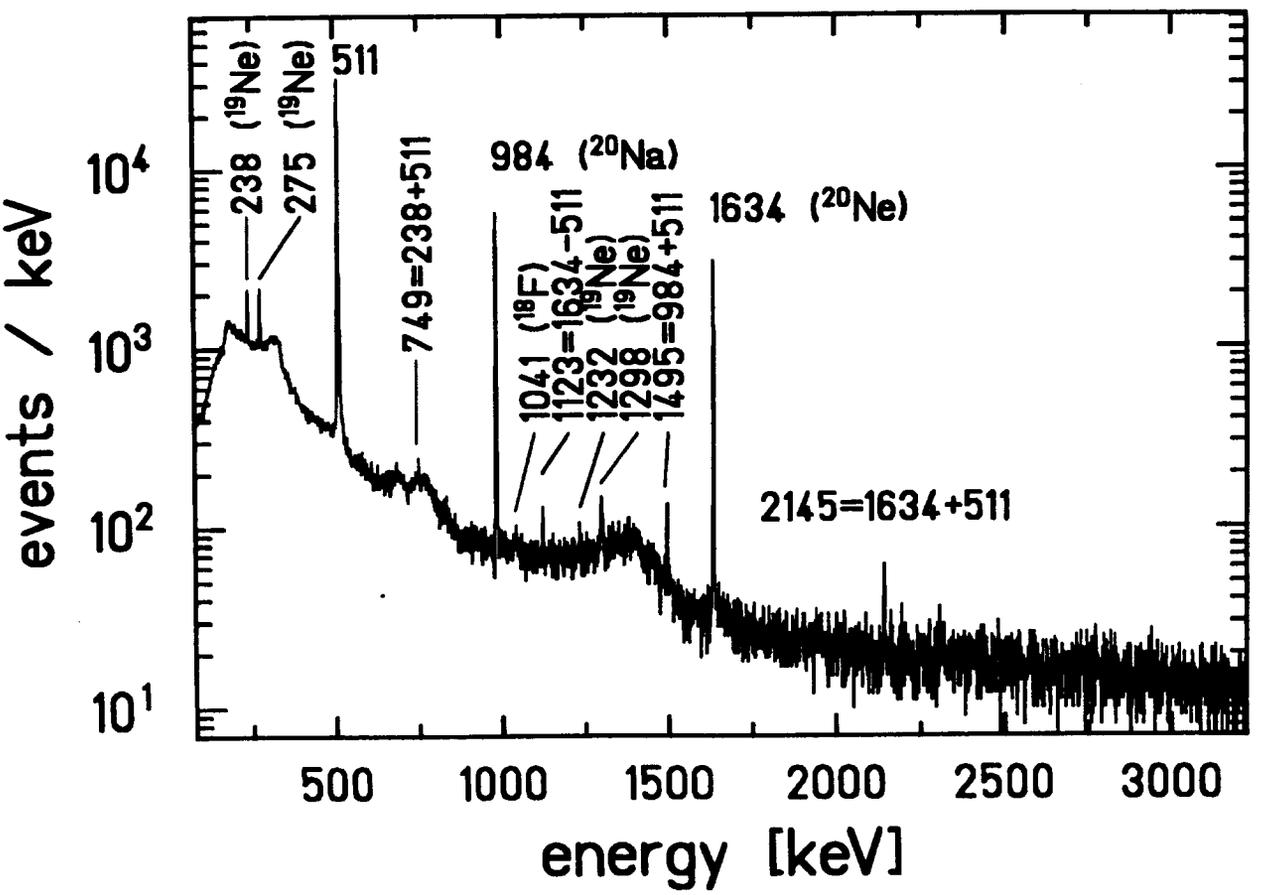

Fig. 6. Energy-spectrum of the $\beta\gamma$-activity from the ^{20}Mg decay chain. The energy of the γ-lines and the γ-ray emitting nuclei are indicated.

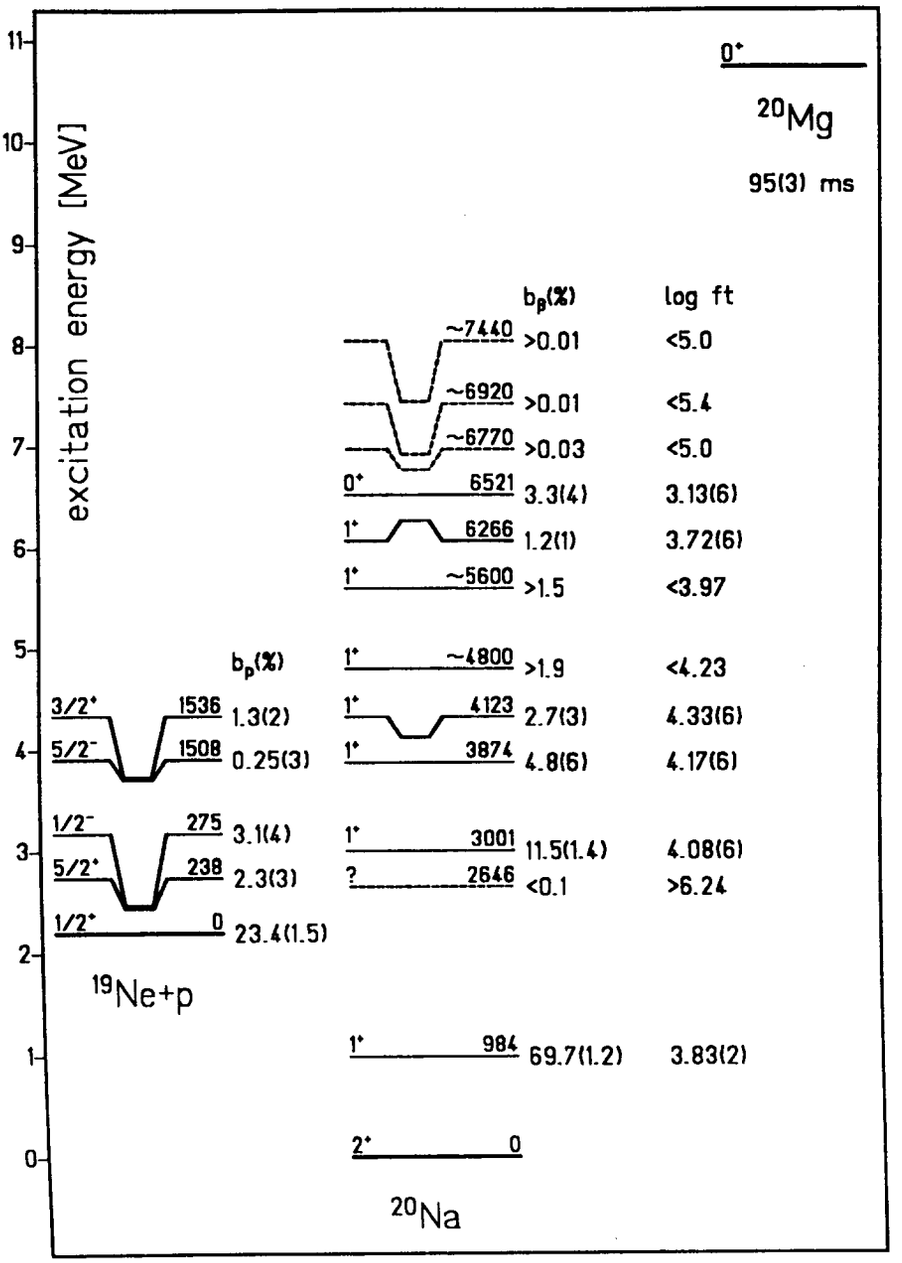

Fig. 7. Partial decay scheme of ^{20}Mg. For the levels populated in ^{20}Na, the level energies, β-decay branching ratios b_β, $logft$-values and J^π-assignments are given. The proton branching ratios b_p to the ^{19}Ne ground-state and to the first four excited states in ^{19}Ne are indicated. All branching ratios are given relative to the number of implanted ^{20}Mg atoms.

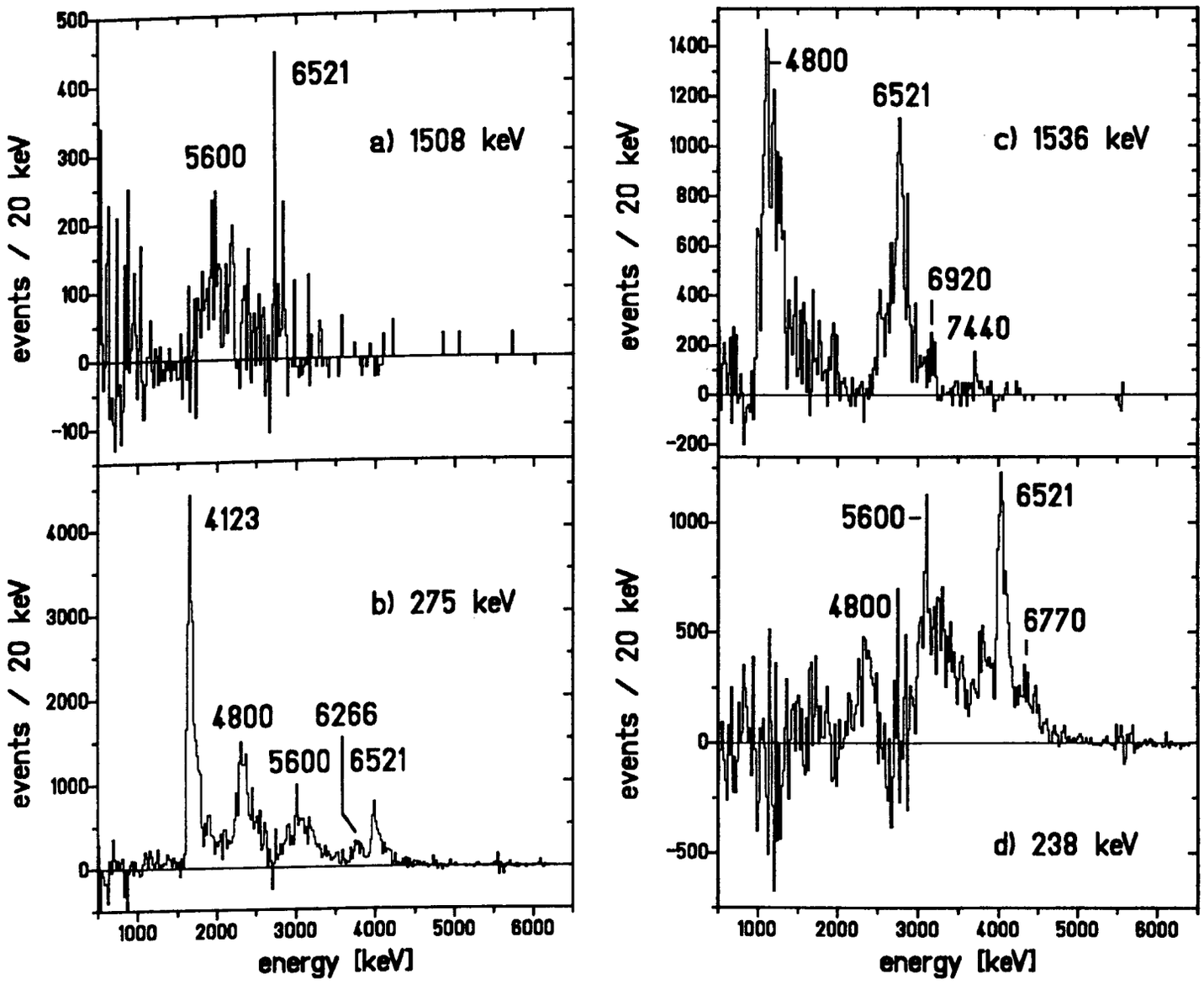

Fig. 8. Energy spectra of β-delayed protons from the ^{20}Mg decay that are emitted in decays to the four excited levels in ^{19}Ne at excitation energies of 238, 275, 1508 and 1536 keV. The abscissa represents the total energy deposited by βp-decays in the implantation detector. The excitation energies of the proton emitting levels in ^{20}Na are indicated.

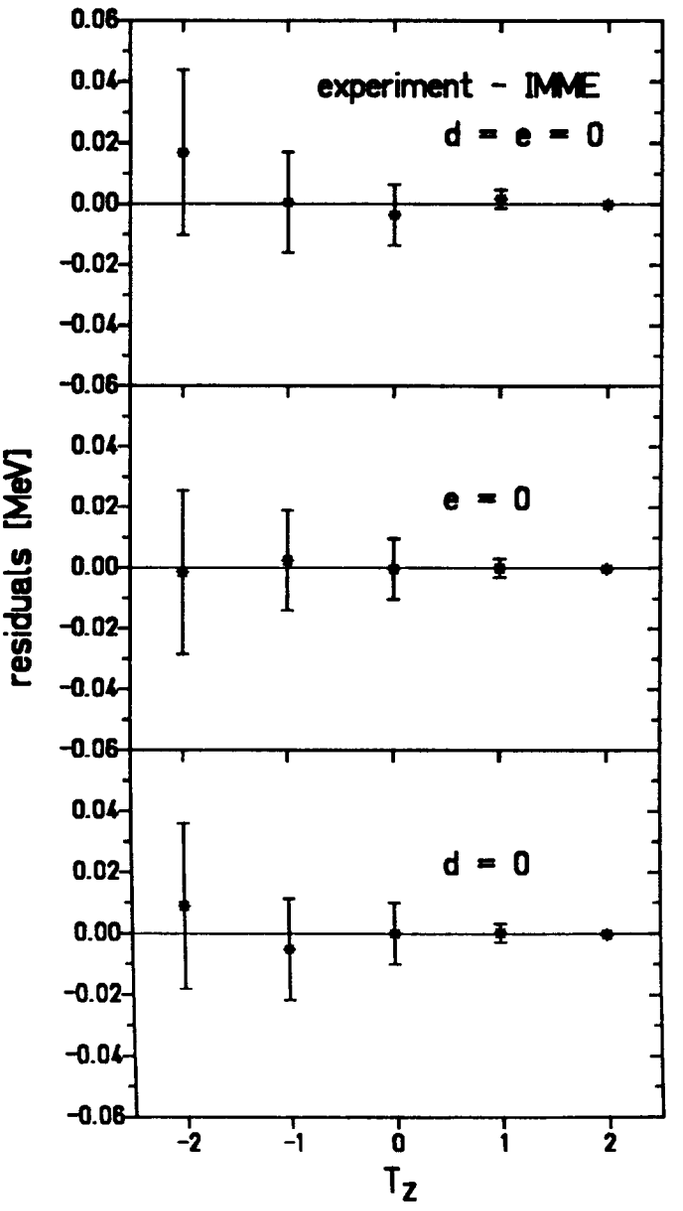

Fig. 9. Differences between experimental masses of the members of the A = 20 isospin multiplet and a polynomial fit $M = a + b \times T_Z + c \times T_Z^2 + d \times T_Z^3 + e \times T_Z^4$. The restrictions imposed on the coefficients d and e are indicated.

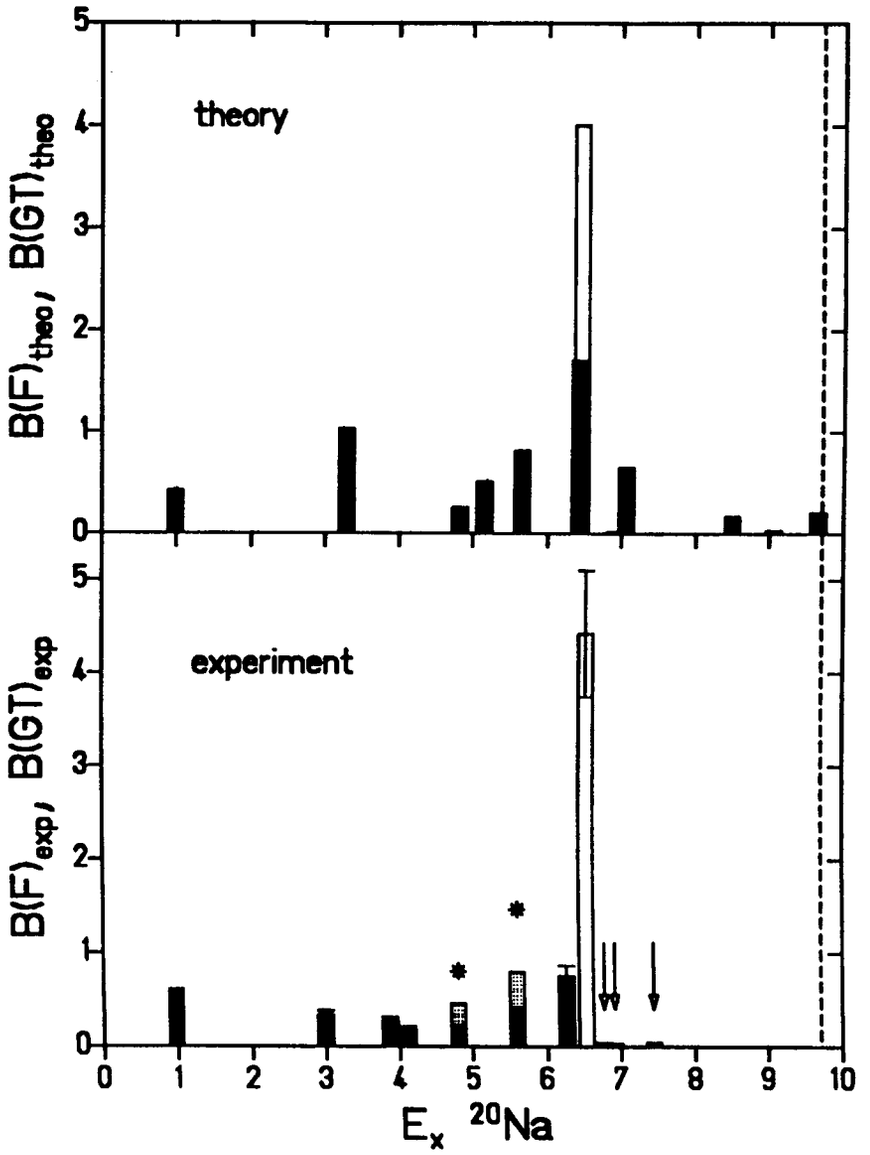

Fig. 10. Calculated (upper panel) and experimental (lower panel) distribution of Fermi- (open bars) and Gamow-Teller (full bars) strength. The asterisk symbols indicate groups of levels which are either broad or unresolved, the arrows levels for which only a lower limit for B(GT) could be determined. The hatched area at the levels of 4800 and 5600 keV represents the estimated distribution of 3% proton-branching to the ^{19}Ne ground state (see text). The dashed line below 10 MeV excitation energy denotes the Q_{β^+}-value limit of the β^+-decay of ^{20}Mg.